

On the Evolution of Trailing Vortex Sheets

M. MOKRY AND A.F.K. YEUNG

Institute for Aerospace Research, NRC, Ottawa, Canada, K1A 0R6
mirek.mokry@nrc.ca and AYeung.MBA2000@ivey.uwo.ca

Abstract

The initial phase of the evolution of trailing vortex sheets is modelled using the continuous sheet method, corresponding to $Re = \infty$. In the proposed 2D numerical scheme, vorticity is conserved. A qualitative comparison of the numerically simulated results and low-speed data obtained by particle image velocimetry is provided. Among the phenomena discussed are the interactions of the trailing vortices with atmospheric and ground shear layers.

1 Introduction

Based on an extensive literature survey and analyses of representative (Memphis airport) data, Sarpkaya¹ draws attention to the fact that there are major problems to understanding the physics of wake vortices. He proposes that: (a) the effects of the molecular diffusion on the demise of trailing vortices is inconsequential, (b) the vortex core is not a benign solid body in rotation, (c) large flow structures are stretched by velocity gradients induced by vortex cores, (d) acquisition of detailed turbulent kinetic energy, dissipation and axial velocity data must be given priority in future experiments and, (e) enhancement of the decay of the vortices is possible through intensification of turbulence near the core and outer instabilities.

Assuming premise (a) to be valid, the present paper examines various aspects of propositions (b) and (c) in the initial stage of the vortex sheet roll-up. The numerical simulation presented here is based on the continuous sheet model². The main advantages of this method over the commonly used discrete vortex method^{3,4} is that the corners of the segmented vortex sheet are 'less' singular than isolated point vortices and that a jump of tangential velocity across the sheet is properly modelled. Consequently, when the sheet rolls up into a spiral, velocity distribution similar to that observed experimentally can be obtained. As observed already by Prandtl and Tietjens⁵, *the connection between vortex motion and the surfaces of discontinuity of potential motion lies in the fact that any small internal friction changes the discontinuity in velocity into a gradual transition in a layer with rotation. In the domain in which this continuous change takes place we have a layer of vorticity formed out of vortex filaments, whereas outside the layer there is potential flow.*

Mathematically, a line of tangential discontinuity is absolutely unstable⁶ and tends to disintegrate into a row of vortices. However, contrary to the discrete vortex method, the descendant vortices are not arbitrarily located point singularities, but rather finite-size structures that effectively increase the thickness of the original vortex sheet. Since stretching (elongation) has a stabilizing effect^{7,8}, it is possible to simulate numerically a fairly regular evolution of vortex sheets by selecting sufficiently small time steps. Techniques such as smoothing, insertion and redistribution, which are known to produce almost perfect vortex spirals⁹, have not been applied.

In an earlier study¹⁰ it has been demonstrated that the mechanism for generating secondary vortices is a local contraction of the sheet accompanied by a rapid peaking of the vortex density

function. The susceptibility of the contraction portions of the sheet to disintegration into smaller secondary vortices is, similarly, related to the spiral-type breakdown of the vortex.

2 PIV experiment

A valuable insight into the internal structure of a vortex wake has been provided by particle image velocimetry (PIV). Since this method is capable of capturing an entire cross-section of the unsteady flowfield at a single time instant, it is more suitable for global investigation of vortex flows than the point-measurement techniques such as the hot wire anemometry, laser Doppler velocimetry, or pressure probes.

Fig.1 is a schematic diagram of a PIV system for measuring wing tip vortices in a wind tunnel. An actual view of a floor-mounted wing and the PIV camera in the IAR 9m x 9m Low Speed Wind Tunnel is shown in Fig.2. The rectangular NACA 0015 wing is of chord length 0.356 m and semi-aspect ratio 4.29. Localized seeding was provided by a smoke generator that continuously ejected vapourised bayoil into the settling chamber, upstream of the model. A double-pulsed Nd:YAG laser coupled with an optical system produced a light sheet of constant thickness that crossed the stream approximately 10 chord lengths downstream of the wing trailing edge.

The PIV image in Fig.3 has been taken with the Dantec DoubleImage CCD camera. It captures a perfectly circular eye of the vortex and the turbulent structure of the shear layer winding around it. However, a word of caution is in place: because of seeding non-uniformity, stream fluctuations, and general unsteadiness of vortex flows, images obtained at longer intervals (say seconds) apart are vastly different, revealing the chaotic nature of the mixed smoke-air flow. In some images, because of a less favourable particle distribution, the vortex spiral is barely discernible while in others some previously hidden flow patterns are revealed. Nevertheless, at wind speeds of about 10 m/s any two images corresponding to light pulses $400\mu\text{s}$ apart still look very much alike. This allows evaluating the velocity vectors on a grid, using local cross-correlation of particles in an 'interrogation' area surrounding each grid point.

A typical example, corresponding to the smoke image in Fig.3, is shown in Fig.4. The PIV processing reveals that the wing tip vortex is located in a highly perturbed flow environment, surrounded by a number of smaller peripheral vortices. In the absence of detailed quantitative comparisons between the experiment and computations, the purpose of including Fig.4 here is merely to suggest certain conditions that should be met by numerical simulations. Based on observation, the velocity is expected to decrease towards the vortex centre in a fairly monotonic fashion and be nonsingular. The commonly used discrete vortex method clearly violates this condition: the velocity becomes infinite in the limit of approaching each isolated point vortex. The continuous sheet method, discussed in this paper, is far more accommodating: the (tangential) velocity merely undergoes a finite discontinuity on crossing the vortex sheet. Admittedly, only the quantitative comparisons with PIV or other measurement data can tell how well the method performs in other respects, for example if the calculated velocity distribution resembles the velocity field inside a viscous vortex core or not.

Further details about the conducted PIV vortex experiment can be found in Refs.11 and 12.

3 Description of the numerical method

The complex velocity induced by the vortex sheet is represented by a line distribution of vorticity

$$w(z) = \int_C \frac{i\gamma(\zeta)}{2\pi(\zeta - z)} |d\zeta| \equiv \frac{1}{2\pi i} \int_C \frac{f(\zeta)}{\zeta - z} d\zeta, \quad (1)$$

where $|d\zeta|$ is the arc length element of the sheet C and γ is the real-valued vortex density function. The complex contour element can be expressed as

$$d\zeta = |d\zeta|[-\sin \nu(\zeta) + i \cos \nu(\zeta)] = |d\zeta| i e^{i\nu(\zeta)},$$

where ν is the angle between the real axis and the normal to C , pointing to the right, see Fig.5. Accordingly, the Cauchy density f is given by

$$f(\zeta) = i\gamma(\zeta)e^{-i\nu(\zeta)}. \quad (2)$$

If z is a point of the vortex sheet C , the complex velocity is calculated by taking the principal value of the integral. This is consistent with the discrete vortex formulation, where the vorticity of a given point does not directly influence its own motion.

The Cauchy-type integral of Eq.(1) describes a function which is analytic everywhere except across C . In accordance with the Plemelj formula,

$$w^+(\zeta) - w^-(\zeta) = f(\zeta), \quad (3)$$

where the superscripts $+$ and $-$ designate the limiting values of w to the left and right of C , respectively. Along C , as may further be verified from the appropriate velocity triangles,

$$w(\zeta) = [v_n(\zeta) - iv_t(\zeta)] e^{-i\nu(\zeta)}, \quad (4)$$

where v_n and v_t are the normal and tangential velocities respectively. Using Eqs.(2-4), it follows for the differences of normal and tangential velocities across the sheet

$$v_n^+(\zeta) - v_n^-(\zeta) = 0 \quad \text{and} \quad v_t^+(\zeta) - v_t^-(\zeta) = -\gamma(\zeta). \quad (5)$$

Accordingly, the successive crossings of the spiral on approaching the vortex core in the radial direction are accompanied by a decrease of the tangential velocity, like in viscous, rotational flow.

Approximating vortex sheet C by constant-density, straight-line segments,

$$w(z) = \sum_j w_j(z), \quad (6)$$

where, from Eqs.(1) and (2),

$$w_j(z) = \frac{f_j}{2\pi i} \int_{\zeta_{j-1}}^{\zeta_j} \frac{d\zeta}{\zeta - z} = \frac{i\gamma_j}{2\pi} \frac{\zeta_j^* - \zeta_{j-1}^*}{|\zeta_j - \zeta_{j-1}|} \ln \frac{\zeta_j - z}{\zeta_{j-1} - z}. \quad (7)$$

The asterisks indicate the complex-conjugate values. If z is an interior point of the segment ζ_{j-1}, ζ_j , the corresponding principal value is¹³

$$w_j(z) = \frac{i\gamma_j}{2\pi} \frac{\zeta_j^* - \zeta_{j-1}^*}{|\zeta_j - \zeta_{j-1}|} \ln \left| \frac{\zeta_j - z}{\zeta_{j-1} - z} \right|. \quad (8)$$

The effect of crosswind or external boundaries can be accounted for by appending an analytic function $F(z)$ to the integrals of Eq.(1). Thus for uniform crosswind,

$$F(z) = v_x = \text{real constant.} \quad (9)$$

For the ground at $y = y_g$,

$$F(z) = \sum_j \tilde{w}_j(z), \quad (10)$$

where the contribution of the j th segment image is obtained from Eq.(7), replacing ζ by $i2y_g + \zeta^*$ and γ by $-\gamma$:

$$\tilde{w}_j(z) = \frac{-i\gamma_j}{2\pi} \frac{\zeta_j - \zeta_{j-1}}{|\zeta_j - \zeta_{j-1}|} \ln \frac{i2y_g + \zeta_j^* - z}{i2y_g + \zeta_{j-1}^* - z}. \quad (11)$$

A shear layer, which in the limit of zero thickness becomes a surface of discontinuity at $y = y_s$, has yet to be treated as an additional vortex sheet. Assuming that the segment endpoints are numbered as shown in Fig.6: on the trailing sheet from 0 to m and on the shear layer from $m+1$ to n , the combined complex velocity can be evaluated as

$$w(z) = \sum_{j=1}^m w_j(z) + \sum_{j=m+2}^n w_j(z) + \psi(z). \quad (12)$$

The isolated term $\psi(z)$ in Eq.(12) is the end effect of the semi-infinite vortex sheet segments on the left of ζ_{m+1} and the right of ζ_n . In order to keep $\psi(z)$ finite, both the semi-infinite segments are required to have the same density, denoted here as γ_∞ . Using Eq.(7) and applying the appropriate limits, the following result is obtained:

$$\psi(z) = \frac{i\gamma_\infty}{2\pi} \left[\ln \frac{\zeta_{m+1} - z}{\zeta_n - z} + i\pi\epsilon \right], \quad \epsilon = \begin{cases} 1, & y > y_s \\ 0, & y = y_s \\ -1, & y < y_s. \end{cases} \quad (13)$$

Initially, when $\eta_j = y_s$, $j = m+1, \dots, n$, and $\gamma_j = \gamma_\infty$, $j = m+2, \dots, n$, the complex velocity induced by the shear layer is

$$\sum_{j=m+2}^n w_j(z) + \psi(z) = -\frac{1}{2}\gamma_\infty\epsilon.$$

In the subsequent evolution of the shear layer it is assumed that the endpoints ζ_{m+1} , ζ_n remain fixed and $\psi(z)$ is invariant.

4 Time stepping

The evolution of the discretized vortex sheet is investigated in the Lagrangian way, by tracing the displacements of segment endpoints in pseudo-time τ . To bypass the logarithmic singularities introduced by segmenting the contour, the velocities at segment endpoints are evaluated as the averages of those at the surrounding midpoints.

The relationship between the pseudo-time and the actual time is dependent upon the definition of the vortex density γ in Eq.(1). We assume the spanwise circulation about the wing to be represented by the sine expansion¹⁴

$$\Gamma(x) = 2bU \sum_{n=1}^{\infty} A_n \sin n\theta, \quad \theta = \arccos \frac{2x}{b}, \quad -\frac{b}{2} < x < \frac{b}{2}, \quad (14)$$

where x is the spanwise coordinate, b is the wing span, and U is the aircraft velocity. From the lifting line theory,

$$A_1 = \frac{C_L}{\pi AR},$$

where C_L is the lift coefficient and AR is the wing aspect ratio. Accordingly, the non-dimensional vortex density is defined as

$$\gamma(x) = -\frac{\pi AR}{UC_L} \frac{d\Gamma(x)}{dx} = 4 \sum_{n=1}^{\infty} na_n \frac{\cos n\theta}{\sin \theta}, \quad (15)$$

where

$$a_n = \frac{\pi AR}{C_L} A_n \quad (a_1 = 1). \quad (16)$$

In this way the equivalence of the roll-up for wings having the same spanwise loading at different lift coefficients and aspect ratios can be exploited. However, since then the velocity described by Eq.(1) is also non-dimensional, the pseudo-time τ must furnish the length dimension. From Eq.(15) it can be deduced that the actual time and corresponding downstream distance are given by

$$t = \frac{\pi AR}{UC_L} \tau \quad \text{and} \quad d = Ut = \frac{\pi AR}{C_L} \tau. \quad (17)$$

For instance, if τ is measured in wing-span units, so is d .

5 VSR examples

The numerical examples given in this paper were produced by code VSR (Vortex Sheet Rollup), written for Windows 95/98 or NT using the Object Windows Library (OWL) of Borland C++, Version 5.02. The code, which was also used to animate vortices at the Third International Workshop on Vortex Flows and Related Numerical Methods (Toulouse, 1998), is attached for the reader's convenience as an **.exe* file.

Fig.7 presents three overlapped windows illustrating the encounter of trailing vortices with an atmospheric (cross-wind) shear layer. Initially, the shear layer divides the plane into the upper half with cross-wind and the lower half with no wind. The computation is started 'impulsively' by inserting a flat trailing vortex sheet of the flying-by aircraft. The positive vortex sheet segments are drawn in blue and the negative ones in purple; 'Time' is the pseudo-time measured in wing span units. From the sequence of the pictures it is seen that the descending aircraft vortices first indent the shear layer and then pass through it. The torn ends of the shear layer (highly stretched segments having the density below a prescribed level are not plotted) are seen to roll up and interact with the aircraft trailing vortices. The tilt of the vortices on passing through the shear layer makes them descend along oblique paths well into the still air below the shear layer. Earlier,

this effect has been ascribed¹⁵ in part to the inertia of air mass inside the vortices, but here the description is purely kinematic.

Using the same method, it has also been confirmed that if the shear layer is sufficiently intense, the downwind aircraft vortex may interact with its oppositely-oriented shear layer counterpart in such a way that the vortices may propel each other upwards¹⁵. In contrast, the equally oriented upwind vortices were found to orbit about each other near the shear layer altitude.

The interaction of the trailing vortices with the shear layer in the vicinity of ground is modelled using the ground images of both the trailing sheet and the shear layer. The strength of vortices and shear layer in Fig.8 are the same as those in Fig.7, but the difference in the two flow patterns is readily apparent. A portion of the shear layer, scooped by the downwind vortex, rolls up into a vortex of opposite orientation. The mutual interaction makes the trailing vortex rise and the weaker shear layer vortex orbit about the former. The path of the trailing vortex is wavy but non-periodic, because the scooping of the shear layer is a continuing process.

The upwind vortex is in this case practically stalled over the runway, acting as a barrier for the advancing shear layer. The resulting contraction of the upwind portion of the shear layer makes it Helmholtz-unstable, that is forcing it to disintegrate into a row of ground-level vortices. As mentioned earlier, in the numerical scheme employed here, vorticity is conserved and vortex sheets are continuous at all times. For esthetic reasons, the highly stretched vortex line segments are not plotted, but they are always accounted for in the computation.

In both Figs.7 and 8 the velocity field has been mapped on a rectangular grid using green vectors. The velocity is seen to decrease from its maximum near the vortex spiral outer boundary towards the centre of roll-up, which is in qualitative agreement with the experimental data of Fig.4. In fact, the available velocity matrices, either measured or computed, can be used as initial conditions for subsequent viscous-flow calculations over longer time intervals.

6 Concluding remarks

It has been shown that a number of phenomena related to the evolution of aircraft trailing vortices, previously observed experimentally or by viscous-flow calculations, can in a simplified form be modelled by the motion of surfaces of discontinuity in potential flow. Among those are the encounters of trailing vortices with atmospheric and ground shear layers. The easy implementation and computational efficiency of the method make it a near-term candidate¹⁶ for a real-time forecasting of aircraft trailing vortices that can be integrated in an airport vortex warning system.

Although the described numerical algorithm is based on an (axiomatically) correct mathematical formulation and the obtained results appear believable, the method is only an approximation, mimicking the true physics. Clearly, more experimental work on the vortex near- and far-field is required in order to test and further develop the method to make it a useful prediction tool. As always, the relevance of two-dimensional modelling should be questioned, particularly in regard to the effects of the axial velocity component and three-dimensional instabilities.

7 Acknowledgments

This project has been supported by the Institute for Aerospace Research under the Vortex Dynamics Program. The authors are obliged to Ben Lee for his helpful suggestions. Gratefully acknowledged is also the assistance of two enthusiastic summer students, Katie Leong and Ian Brown, in setting up and running the wind tunnel experiment in June of 1997.

8 References

- ¹SARPKAYA, T.: Decay of Wake Vortices of Large Aircraft. *AIAA Journal* **35** (1998) 1671-1679.
- ²MOKRY, M. and RAINBIRD, W.J.: Calculation of Vortex Sheet Roll-up in a Rectangular Wind Tunnel. *Journal of Aircraft* **12** (1975) 750-752.
- ³ROSENHEAD, L.: The Formation of Vortices from a Surface of Discontinuity. *Physics of Fluids A* **5** (1933) 170-192.
- ⁴WESTWATER, F.L.: The Rolling Up of the Surface of Discontinuity behind an Aerofoil of Finite Span. R & M 1692 (1935) Aeronautical Research Council, Great Britain.
- ⁵PRANDTL, L. and TIETJENS, O.G.: *Fundamentals of Hydro- and Aeromechanics*. Dover (1957) 216.
- ⁶LANDAU, L.D. and LIFSHITZ, E.M.: *Fluid Mechanics*. Pergamon Press (1959) 115-116.
- ⁷MOORE, D.W. and GRIFFITH-JONES, R.: The Stability of an Expanding Circular Vortex Sheet. *Mathematika* **21** (1974) 128-133.
- ⁸SAFFMAN, P.G.: *Vortex Dynamics*. Cambridge University Press (1992) 152-155.
- ⁹KRASNY, R.: Computation of Vortex Sheet Roll-Up in the Trefftz Plane. *Journal of Fluid Mechanics* **184** (1987) 123-145.
- ¹⁰MOKRY, M.: Real-time Simulation of Aircraft Wake Vortices. Proc. 5th Annual Conference of the CFD Society of Canada, Victoria, BC (1997) 9.14-9.20.
- ¹¹YEUNG, A.F.K. and LEE, B.H.K.: Particle Image Velocimetry Study of Wing-Tip Vortices. *Journal of Aircraft* **36** (1999) 482-484.
- ¹²YEUNG, A.F.K.: The Application of PIV in the IAR 9m x 9m Wind Tunnel. NRC IAR LM-A-030 (1998).
- ¹³GAKHOV, F.D.: *Boundary Value Problems*. Pergamon Press (1966) 1-84.
- ¹⁴KATZ, J. and PLOTKIN, A.: *Low-Speed Aerodynamics*. McGraw-Hill (1991) 207-210.
- ¹⁵PROCTOR, F.H.: The NASA-Langley Wake Vortex Modelling Effort in Support of an Operational Aircraft Spacing. AIAA 98-0589 (1998).
- ¹⁶RENNICK, S.G.: A Transport Canada Perspective. Proceedings of the International Wake Vortex Meeting, Ottawa, Transport Canada TP-13166 (1997) 21-23.

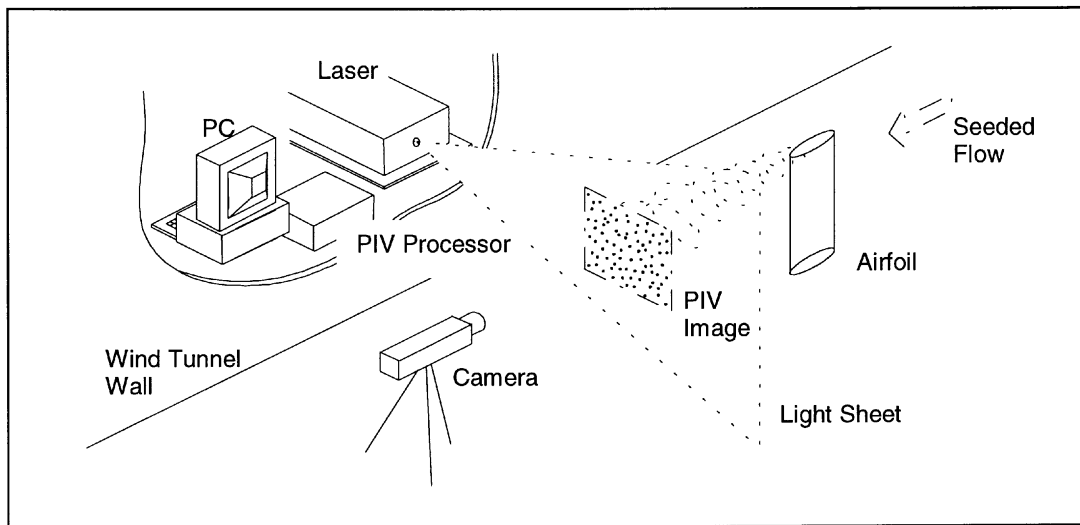


Figure 1: Schematic of the experimental setup

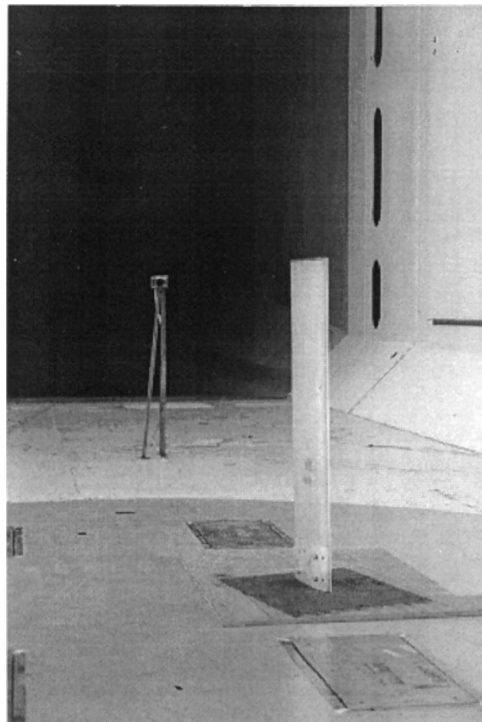


Figure 2: Half-wing and PIV camera in the IAR 9m x 9m Wind Tunnel

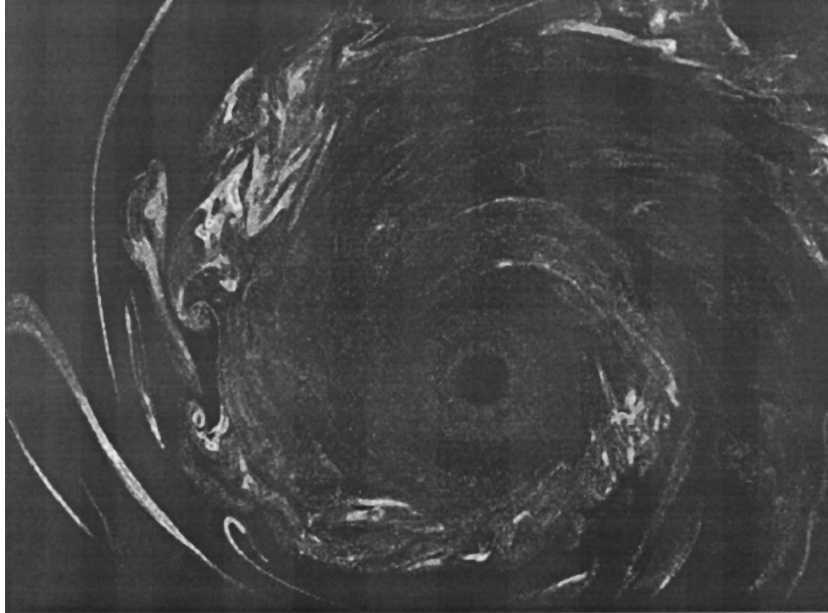


Figure 3: PIV image taken at 6.7m/s, $Re_c = 130000$ and $\alpha = 140^\circ$
Image area: 320mm x 240 mm

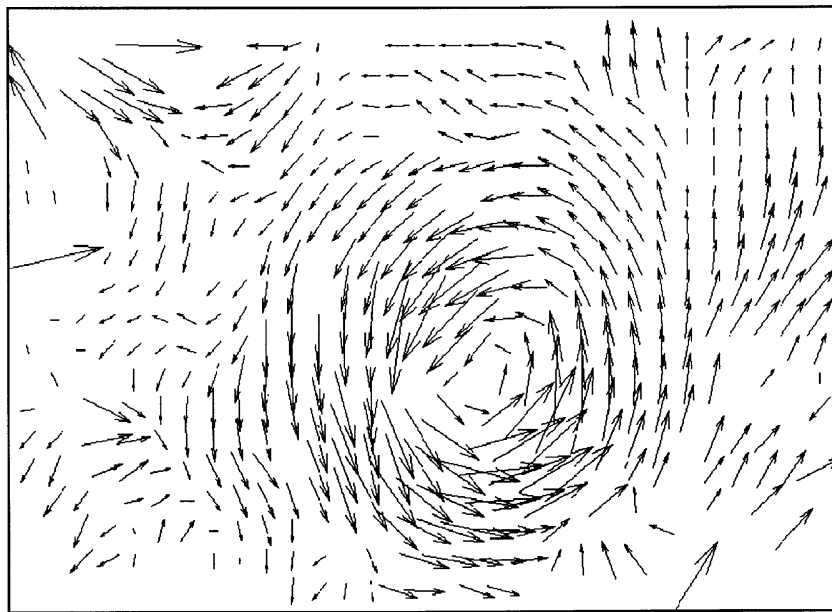


Figure 4: Velocity vector map of Fig.3

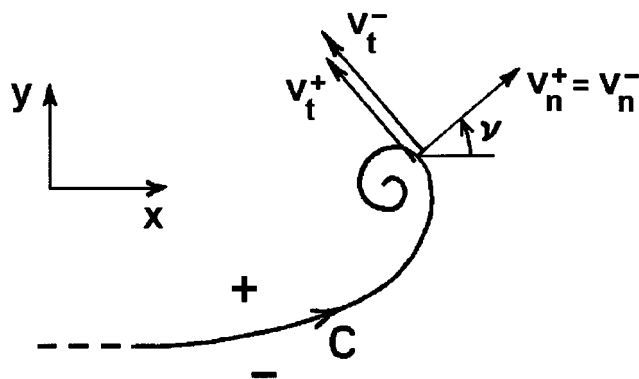


Figure 5: Schematic of a vortex spiral.

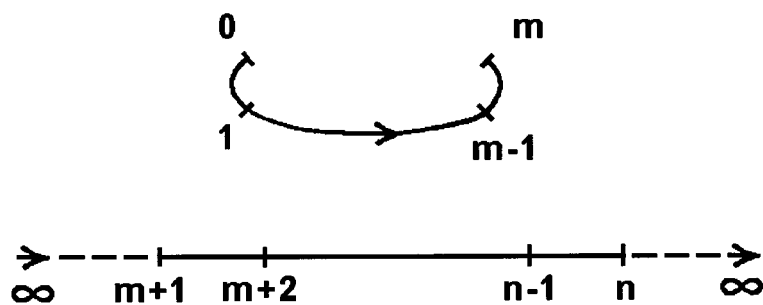


Figure 6: Numbering of segment endpoints.

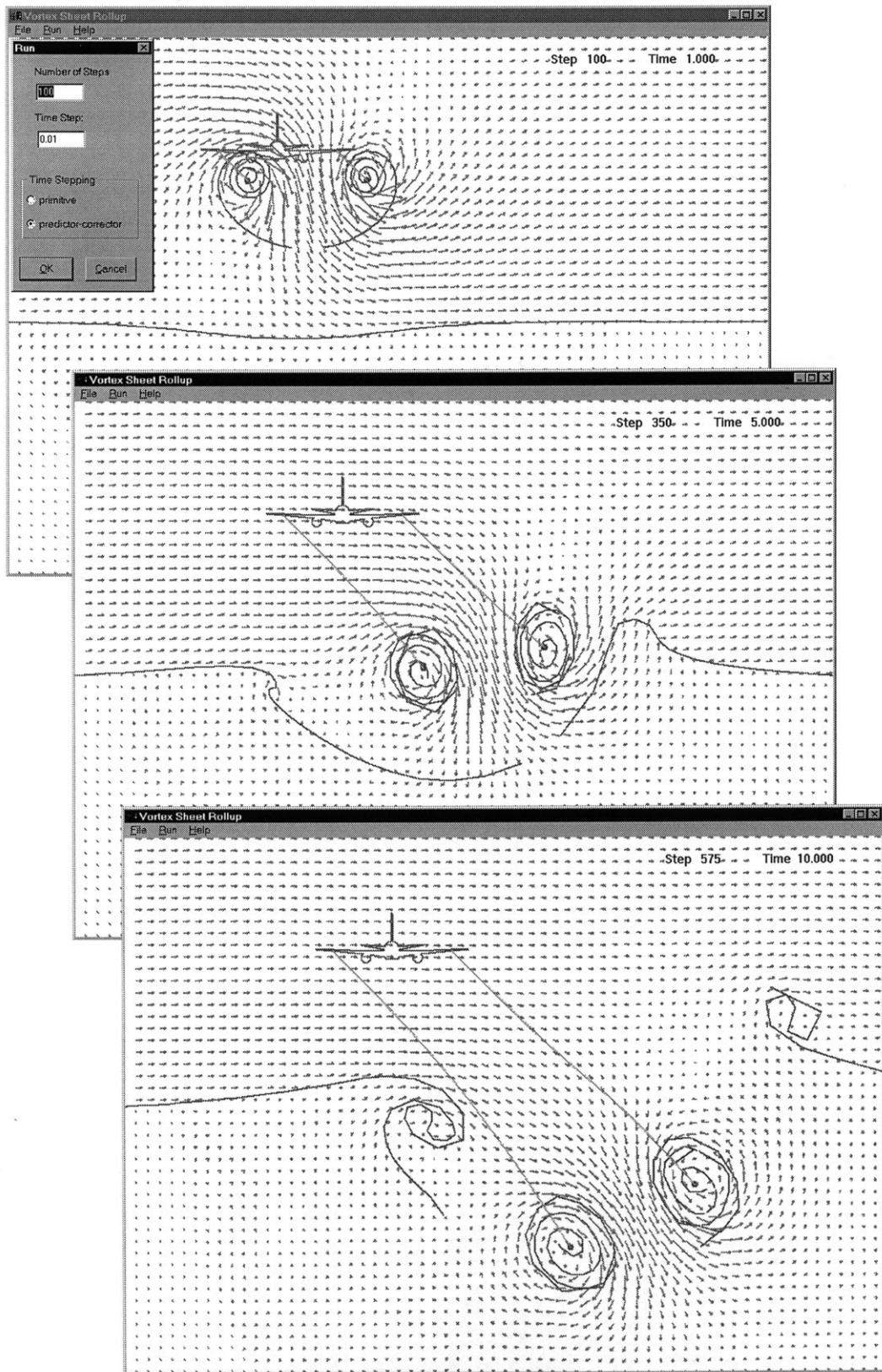


Figure 7: Interaction of trailing vortices and atmospheric shear layer

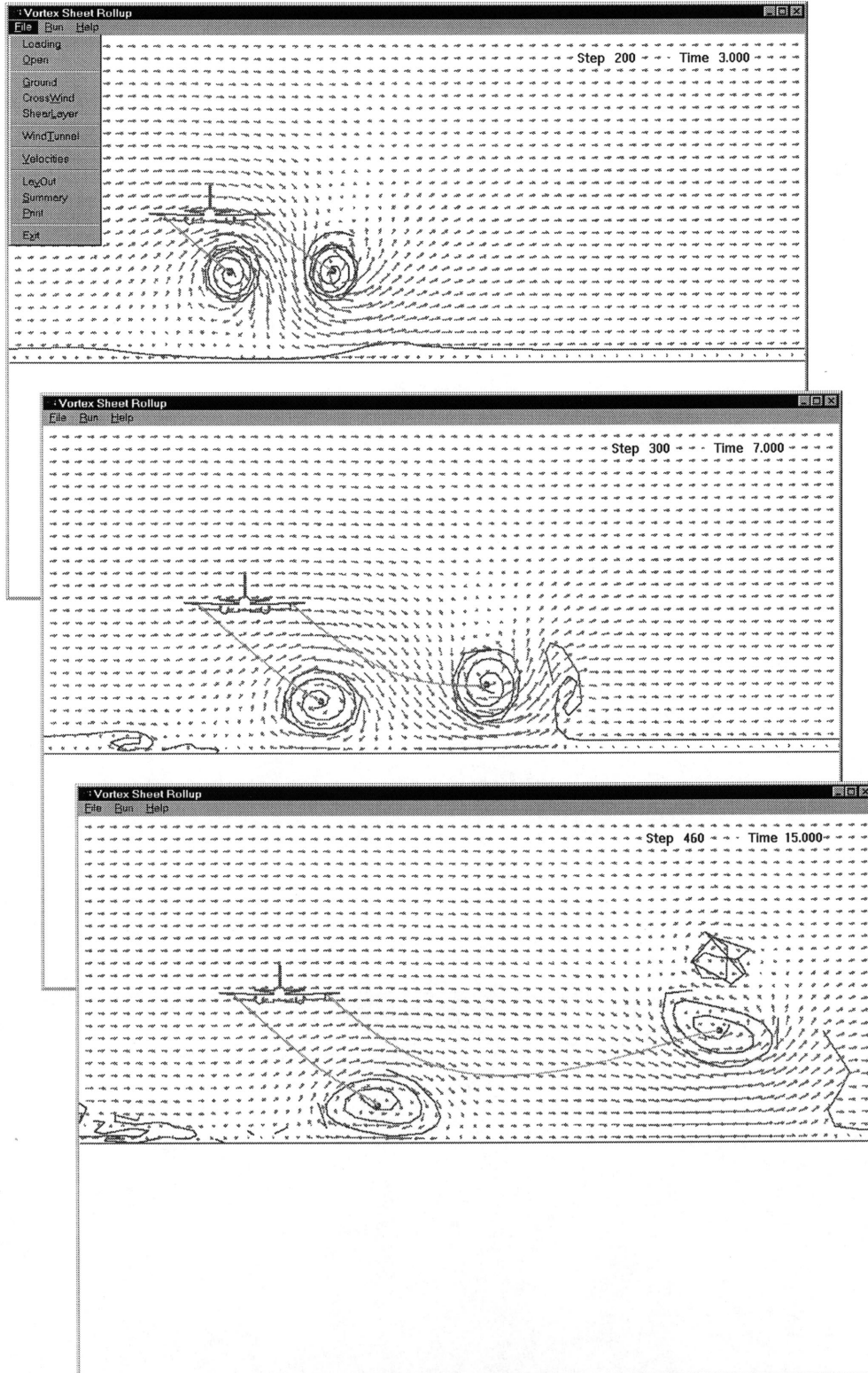


Figure 8: Interaction of trailing vortices and ground shear layer